https://doi.org/10.5194/egusphere-2026-5629
Preprint. Discussion started: 25 September 2026

Using 1 second LEO clock corrections for the Fengyun-3E radio occultation retrievals

Xinyu Zhang[1,2], Wenwu Ding[1,*], Xiangguang Meng[3], Ying Li[1], Yan Liu[4], Yunbin Yuan[1]

[1]State Key Laboratory of Precision Geodesy, Innovation Academy for Precision Measurement Science and Technology, Chinese Academy of Sciences, Wuhan, 430071, China
[2]College of Earth and Planetary Sciences, University of Chinese Academy of Sciences, Beijing, 100049, China
[3]National Space Science Center, Chinese Academy of Sciences, Beijing, 100190, China
[4]Earth System Modeling and Prediction Centre, China Meteorological Administration, Beijing 100081, China

Correspondence to: Wenwu Ding (dingwenwu@apm.ac.cn)

Abstract. Clock offset constitutes a major error source for Global Navigation Satellite System (GNSS) radio occultation (RO) products, particularly for stratospheric observations. The adoption of high-rate clock correction strategy can effectively mitigate clock offset induced errors. In this study, high-rate (1-s) undifferenced (UD) Low Earth Orbit (LEO) clock corrections are used to retrieve RO observations from the Fengyun-3E (FY-3E) satellite. The retrieval results are compared with those derived from the conventional 30-s clock correction scheme and the single-difference (SD) scheme currently adopted in the official data processing. The results demonstrate that the 1-s LEO clock correction scheme improves the overall quality of FY-3E RO retrievals. For bending angle, the most prominent improvements are found in the altitude range of 40-60 km. Globally, its systematic difference is roughly 3% smaller than that of the 30-s scheme and 1% smaller than the SD scheme. Such superiority further propagates downward to refractivity and dry temperature. For refractivity, the largest improvements are also found in the altitude range of 40-60 km with systematic differences for the 1-s UD scheme reduced by approximately 0.5% relative to the other two schemes. Standard deviations of the 1-s scheme remain consistently smaller across the complete height range. Standard deviations of dry temperature are also improved with standard deviations about 0.5% smaller than SD and 1% to 2% smaller than the 30-s scheme in the altitude range from 0-40 km. The results in this study demonstrate the capability of using 1-s clock correction scheme for further promoting Fengyun GNSS Occultation Sounder-II (GNOS-II) RO observations. The results here can provide support for future operational processing and archive reprocessing of all Fengyun GNSS occultation datasets.

1 Introduction

Global Navigation Satellite System (GNSS) Radio Occultation (RO) technique is a robust remote sensing technique for sensing the Earth's atmosphere (Kursinski et al., 1997; Melbourne et al., 1994). It sets RO receivers on Low Earth Orbit (LEO) satellites to receive GNSS signals. As the signals propagate through the atmosphere, they are bent and delayed due to the refractive gradient. Given the orbit information of both GNSS and LEO satellites, the atmospheric delay can be resolved

https://doi.org/10.5194/egusphere-2026-5629
Preprint. Discussion started: 25 September 2026

and subsequent accumulated bending angles can be retrieved (Kursinski et al., 1997; Hajj et al., 2002). Based on bending angle, other atmospheric profiles, such as refractivity, pressure and temperature can all be retrieved (Anthes, 2011; Kursinski et al., 1997; Steiner et al., 2011; Wickert et al., 2005; Wickert et al., 2001). RO data has revealed several distinctive advantages in terms of global distribution, high accuracy (in the upper troposphere and lower stratosphere (UTLS)), high precision and all-weather conditions (Foelsche et al., 2011; Ladstädter et al., 2015; Angerer et al., 2017). Therefore, RO data has been widely used in numerical weather prediction (Healy and Eyre, 2000; Cucurull and Derber, 2008; Huang et al., 2010; Singh et al., 2021), climate monitoring (Steiner et al., 2011; Steiner et al., 2020; Li et al., 2023; Li et al., 2026) and severe weather monitoring (Teng et al., 2023; Yang et al., 2023b). Therefore, RO data can serve as climate-benchmark data (Bosilovich et al., 2013; Parker, 2016; Simmons et al., 2020; Hersbach et al., 2020).

However, above 30 km, the accuracy of RO data is degraded due to the influences of clock offsets, orbit determination and residual ionospheric errors (Li et al., 2013; Li et al., 2015). These errors limit the applications of RO data from middle stratosphere above (Angerer et al., 2017; Li et al., 2021; Li et al., 2023). Among these error sources, clock offsets have been proved to be one of the main error sources of RO observations at high altitudes (Padovan et al., 2025; Yao et al., 2023; Innerkofler et al., 2023). To minimize the impacts of clock offsets on RO products, several measures have been taken. In the early stage, the double-difference (DD) scheme was applied for clock offset correction (Sokolovskiy, 1996; Kursinski et al., 1997; Wickert et al., 2001). Studies demonstrated that this algorithm can effectively mitigate errors caused by GPS/LEO satellite clock offsets through differential processing (Wickert et al., 2002; Melbourne et al., 1994; Beyerle et al., 2005; Schreiner et al., 2010). Following improvements in GNSS clock offset estimation accuracy and rapid progress in precise LEO clock offset determination contributed by the enhanced stability of space-borne oscillators, the single-difference (SD) and undifferenced (UD) methods were gradually adopted in GNSS radio occultation processing for excess phase retrieval (Wickert et al., 2002; Schreiner et al., 2010; Schreiner et al., 2011; Xia et al., 2017). SD processing has become the primary approach since the CHAllenging Minisatellite Payload (CHAMP) mission, while UD processing has emerged as a promising alternative and drawn extensive research attention in recent years. Instead of introducing reference-link observations for removing GNSS/LEO satellite clock offset, these methods directly apply high precision GNSS/LEO clock products for correction. Under this circumstance, the additional errors introduced by reference-link observations are avoided, while the actual correction errors become important.

Besides the errors in the GNSS/LEO satellite clock products, additional errors are introduced when clock products are interpolated to the actual high-rate RO observations epochs, which may further degrade the accuracy of bending angle estimation and subsequent atmospheric products. Therefore, the temporal resolution of GNSS/LEO clock products and corresponding interpolation errors have become important factors influencing RO retrieval performance. Previous studies have investigated UD processing using high-rate LEO clock products with temporal resolutions of 1 s and 2 s for the Constellation Observing System for Meteorology, Ionosphere, and Climate (COSMIC) and COSMIC-2 missions, demonstrating that enhanced temporal resolution of LEO clock products can reduce excess phase rate noise and improve bending angle quality (Xia et al., 2017; Zhang et al., 2022; Guo et al., 2024). Furthermore, comparisons between RO retrievals using 30-s and 2-s GNSS clock products have demonstrated that higher-rate GNSS clock products can also reduce bending angle estimation uncertainty and further improve RO retrieval performance (Yao et al., 2025). These achievements demonstrated the value of high-temporal-resolution satellite clock products in GNSS RO processing.

However, there are still several issues that have not been addressed. First of all, a direct comparison between 1-s and 30-s LEO clock corrections and their impacts on RO retrieval performance have not been fully investigated. Most existing studies focus on comparing UD and SD clock-correction schemes, whereas the interpolation errors associated with clock corrections have rarely been investigated. Second, prior work has predominantly examined RO quality improvements in the UTLS region enabled by high-rate LEO clock products. However, as demonstrated in existing studies (e.g., Zhang et al., 2022), the improvements introduced by clock correction mainly take effect in and above the middle stratosphere. Furthermore, although a small number of studies have discussed the feasibility of UD processing using 30-s clock products from the GNSS Occultation Sounder-I (GNOS-I) receiver, the feasibility of employing 1-s clock products from the GNOS-II receiver remains unexplored.

In this study, we systematically compare the effects of three different clock correction schemes, i.e., 1-s clock correction, 30-s correction and the SD method, on the retrieval quality of RO products from the Fengyun-3E (FY-3E) GNOS-II receiver. The RO atmospheric profiles derived from the three clock schemes are cross-compared and further validated against the European Centre for Medium-Range Weather Forecasts (ECMWF) Reanalysis v5 (ERA5) reanalysis datasets. The quantitative evaluation and comparative analysis clarify the altitude-dependent impacts of clock correction strategies on RO inversion accuracy. It is expected that the conclusions obtained in this work can provide reliable technical references and effective optimization guidance for the operational real-time processing and historical archive reprocessing of all Fengyun satellite GNSS occultation datasets in future studies.

2 Data and methodology

2.1 Data

This study employs GPS RO observations from the FY-3E GNOS-II receiver. The dataset spans 14-16 July 2023 and includes 1027 GPS RO events in total: 347 on 14 July, 335 on 15 July, and 345 on 16 July, averaging approximately 342 events per day. In addition to RO measurements, precise orbit determination (POD) data from the FY-3E GNOS-II payload are used to derive precise orbits and estimate LEO receiver clock offsets. The Center for Orbit Determination in Europe (CODE) GNSS precise orbit and clock products serve as the reference for transmitter-side GPS satellite orbits and clocks. Using these input datasets, a consistent set of FY-3E orbit products and a 1-s receiver clock correction time series were generated. The 30-s clock correction series was produced by sampling the 1-s series at 30-s intervals, followed by linear interpolation to the 1-s occultation epochs.

To assess the quality of RO profiles retrieved under different clock correction schemes, ERA5 dataset is adopted for intercomparison (Hersbach, 2019; Hersbach et al., 2020; Simmons et al., 2020). ERA5 replaced ERA-Interim as the

https://doi.org/10.5194/egusphere-2026-5629
Preprint. Discussion started: 25 September 2026

operational ECMWF reanalysis from August 2019 onwards. Built using state-of-the-art data assimilation methods, ERA5 assimilates a wide range of atmospheric observations and provides hourly gridded outputs. It has a horizontal resolution of about 30 km with 137 vertical levels, covering altitudes from the surface up to approximately 80 km. The ERA5 dataset was vertically interpolated to regular grids and further transformed into bending angle space by the Wegener Center for Climate and Global Change (WEGC), University of Graz.

2.2 RO data retrieval

The RO retrieval workflow, as shown in Fig. 1, comprises four sequential processing steps. The first step involves POD and receiver clock offset estimation. Steps 2 to 4 sequentially perform excess phase calculation, bending angle inversion, and refractivity and dry temperature inversion. Three independent processing schemes are established for intercomparison: UD processing using 1-s LEO receiver clock corrections, UD processing adopting 30-s clock corrections, and the SD scheme currently implemented in operational Fengyun RO data processing. Since identical inversion algorithms are adopted for all schemes, discrepancies among retrieved products stem solely from differences in clock-correction strategies.

In the first step, the precise FY-3E orbit and clock offset products were estimated using the Bernese GNSS Software based on observations collected by the POD antenna (Dach et al., 2015). The final reduced-dynamic orbit and high-rate receiver clock offset products were subsequently generated using the processed POD observations (Kang et al., 2006; Hwang et al., 2009; Jaeggi et al., 2021; Weiss, 2021; Kong et al., 2022). The GNOS-II payload is equipped with three independent antennas for rising occultation, setting occultation, and POD measurements, respectively. The estimated receiver clock offsets correspond to the POD observation channel used in the orbit determination. Differential hardware delays between the POD and forward/backward occultation channels, provided by the National Space Science Center (NSSC), were then applied to obtain clock corrections for RO observations.

In the second step, the excess phase is calculated based on FY-3E GNOS-II RO observations. First, raw L1 and L2 carrier-phase measurements are preprocessed via cycle-slip detection and repair. The precise orbit and clock products of FY-3E, together with the CODE GNSS precise orbit and clock datasets, are used to calculate the instantaneous geometric range between GPS and FY-3E at each occultation epoch, where relativistic corrections are rigorously incorporated into the excess phase derivation. For the two UD processing schemes, L1 and L2 carrier phases are combined to construct ionosphere-free observables. After removing the geometric range term and GPS satellite clock offsets, 1-s and 30-s FY-3E receiver clock corrections were linearly interpolated to the RO observation epochs and directly applied to generate the corresponding UD excess phase products. In contrast, the SD scheme adopts a concurrently observed non-occulting GPS satellite as the reference link to eliminate FY-3E receiver clock offsets. The reference satellite is selected from non-occulting GPS satellites with continuous dual-frequency coverage throughout the occultation period, with priority given to the satellite with the highest elevation angle relative to the navigation antenna (Yang et al., 2023a). Nevertheless, this differencing procedure inevitably introduces additional observational noise and reference-link residual errors. In this study, the SD-derived excess phase is adopted as the benchmark for quantitative comparison with the UD 1-s and UD 30-s results.

https://doi.org/10.5194/egusphere-2026-5629
Preprint. Discussion started: 25 September 2026

130 The third step retrieves bending angle profiles from the excess phase products. The Radio Occultation Processing Package (ROPP) developed by the Radio Occultation Meteorology Satellite Application Facility (ROM SAF) is used for bending angle calculation (Culverwell et al., 2015; Rom Saf, 2024). The excess phase is differentiated with respect to time using a five-point Lagrange interpolation scheme to obtain the excess phase rate. It is then used to derive the ionosphere-corrected bending angle based on geometric-optics theory (Kursinski et al., 1997; Melbourne et al., 1994). L2 extrapolation is applied
135 where necessary, and height-stratified quality control is subsequently performed to remove abnormal profiles (Liao et al., 2019). The bending angle profiles are further statistically optimized to reduce high-altitude noise and to provide reliable input for refractivity retrievals.

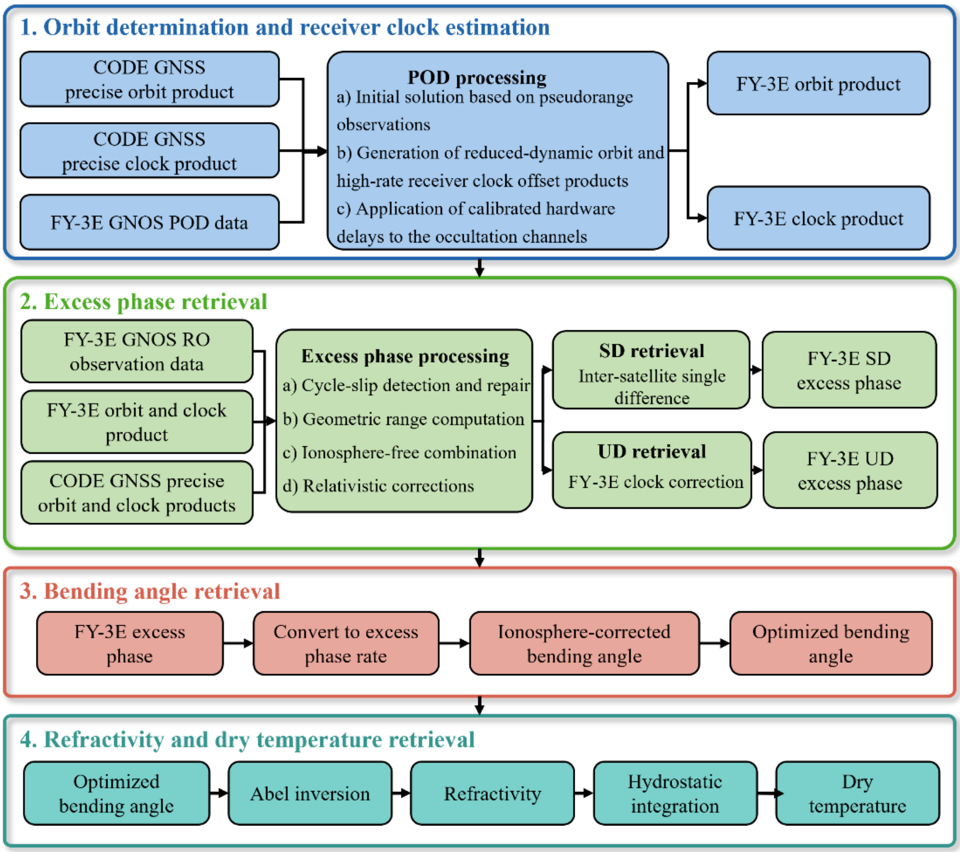

Figure 1: Flowchart of FY-3E GNOS-II radio occultation retrieval

140 The fourth step is to retrieve refractivity and dry temperature from the optimized bending angle. The optimized bending angle is converted into atmospheric refractivity through Abel inversion, which is the standard approach for spherically symmetric RO retrievals (Fjeldbo et al., 1971). The dry temperature profile can then be retrieved using the hydrostatic integration, ideal gas law and the Smith-Weintraub equations (Kursinski et al., 1997; Melbourne et al., 1994). Corresponding quality control schemes are also applied in this step.

2.3 Quality control and evaluation

In order to use high-quality RO profiles and remove the outliers, a quality control strategy is applied in this study to ensure the robustness of profile evaluation (Li et al., 2026). Specifically, three quality control criteria are implemented as follows: (a) For altitudes between 50 and 80 km, a profile is discarded if the absolute difference between the ionosphere-corrected bending angle and the ERA5-derived bending angle exceed ±40 μrad; (b) For altitudes ranging from 35 to 50 km, an occultation event is eliminated when the absolute relative difference between the ionosphere-corrected bending angle and the ERA5 bending angle is larger than 100%; (c) Within the altitude interval of 10-35 km, an event is rejected if any of the following thresholds is violated: bending angle relative difference exceeding 20%, refractivity relative difference exceeding 10%, or absolute dry temperature difference exceeding 10 K. After quality control, a total of 1027 RO events are retained for statistical analysis. Among these samples, there are 502 rising events observed by the forward-looking receiver and 525 setting events measured by the backward-looking receiver.

For statistical evaluation, we calculate the differences between RO profiles and ERA5 reanalysis data, comprising systematic differences and associated standard deviations. These statistical quantities are calculated for ionosphere-corrected bending angles, optimized bending angles, refractivity, and dry temperature. To investigate the latitudinal dependence of such errors, statistics are computed over six separate latitude bands: the global domain (90°S-90°N), Southern Hemisphere mid-latitudes (20°S-60°S), Northern Hemisphere mid-latitudes (20°N-60°N), Southern Hemisphere polar region (60°S-90°S), Northern Hemisphere polar region (60°N-90°N), and the tropics (20°S-20°N).

3 Results and discussion

This section details RO retrieval results obtained using three different clock correction approaches: the 1-s correction, the 30-s correction, and the SD scheme currently implemented in the operational Fengyun RO processing system. Subsection 3.1 analyzes products generated with the 1-s clock correction. Subsection 3.2 addresses excess phase and bending angle results, while Sect. 3.3 describes the corresponding refractivity and dry temperature retrievals.

3.1 1-s clock correction products

To assess how temporal resolution of LEO clock offset affects undifferenced occultation processing for FY-3E, this study compares 1-s and 30-s LEO receiver clock correction products in both the time and frequency domains. Time-domain analysis uses the difference between 1-s and 30-s clock-rate sequences to characterize short-timescale residual variations. For frequency-domain evaluation, the modified Allan deviation (MDEV) is adopted to quantify the stability of distinct clock products over a range of averaging intervals.

Figure 2 shows the detrended clock rate sequences derived from the 1-s and 30-s clock products of the FY-3E fore receiver during the first 6 h of day of year (DOY) 195, 2023. The green and red curves represent the results derived from the 1-s and 30-s clock products, respectively. Both curves exhibit similar short-term (e.g., <30 min) and long-term variation

https://doi.org/10.5194/egusphere-2026-5629
Preprint. Discussion started: 25 September 2026

characteristics. The lower panel further shows the differences between the two clock rate sequences, with a standard deviation of 0.024 ns/s. This result indicates that the 30-s clock product cannot fully recover the short timescale variations contained in the 1-s product, which may affect applications involving high-rate RO observations. It is worth noting that the behavior shown in Fig. 2 is also observed during other time periods and for the aft receiver clock products.

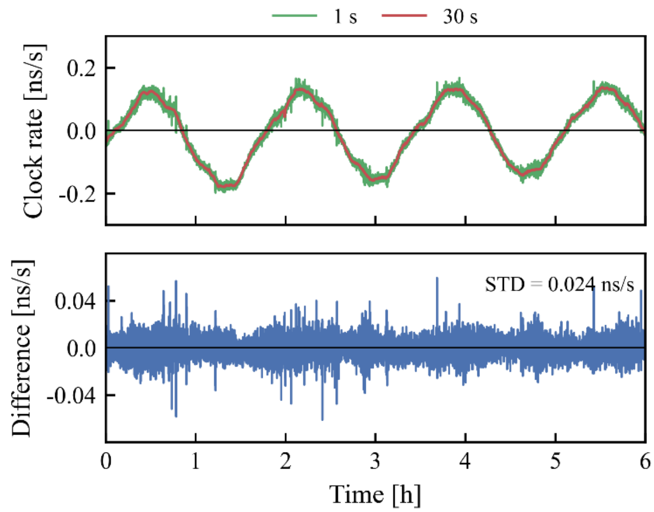

Figure 2: Detrended clock-rate sequences and their differences derived from the 1-s and interpolated 30-s FY-3E forward receiver clock products during the first 6 h of DOY 195, 2023.

Figure 3 evaluates their short-term frequency stability using the MDEV over averaging times from 0.1 s to 10000 s; both series were resampled to 0.1 s beforehand to ensure comparability. The results show that, at τ = 1 s, the frequency stability values of the 1-s and 30-s products are 1.6×10^{-11} and 3.0×10^{-11}, respectively. At τ = 0.1 s, the corresponding values are 1.2×10^{-10} and 2.9×10^{-10}. As the averaging time increases, the difference between the two products gradually decreases. At τ = 1000 s, the 1-s and 30-s products converge to 3.4×10^{-12} and 3.6×10^{-12}, respectively, with a difference of less than 6%.

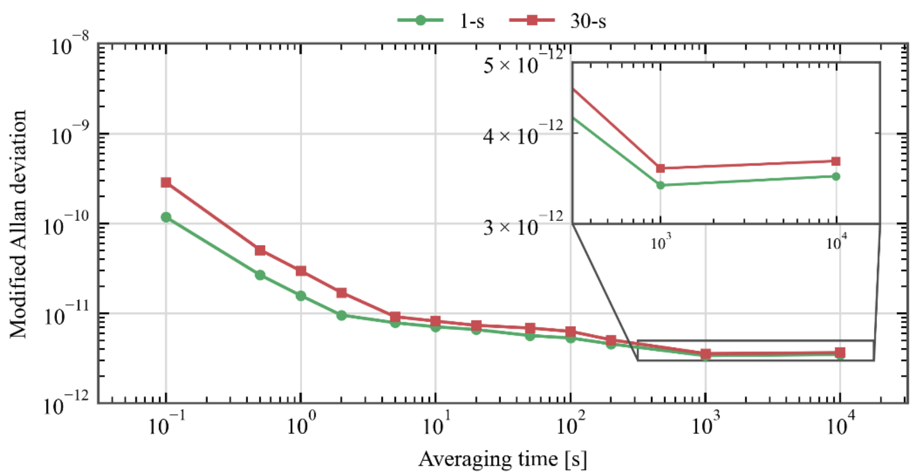

Figure 3: MDEV comparison of FY-3E forward receiver clock corrections for 1-s and 30-s products (DOY 195, 2023).

https://doi.org/10.5194/egusphere-2026-5629
Preprint. Discussion started: 25 September 2026

These results indicate that the 1-s clock series exhibits smaller short-term frequency variations than the downsampled and interpolated 30-s series, particularly at sub-second to several-second averaging times.

3.2 Excess phase and bending angle

Figure 4 shows the excess phase rate for two representative FY-3E RO events across three time windows. Across the full observation period, the excess phase rate from 30-s scheme deviates obviously from the other two schemes starting at 60 s. Within the initial 15 s, the first occultation event yields smaller values than the second event, which implies smaller bending angles during this interval. For the first 15 seconds (middle column panels) and 5 seconds (right column panels), the excess phase rate derived from the 30-s scheme exhibits evidently larger noise levels than the other two schemes. Specifically, the 1-s scheme yields the smoothest excess phase rate, while the SD scheme presents intermediate results between the 1-s and 30-s schemes. In addition, the 1-s and SD schemes show generally better consistency with each other compared with the 30-s scheme.

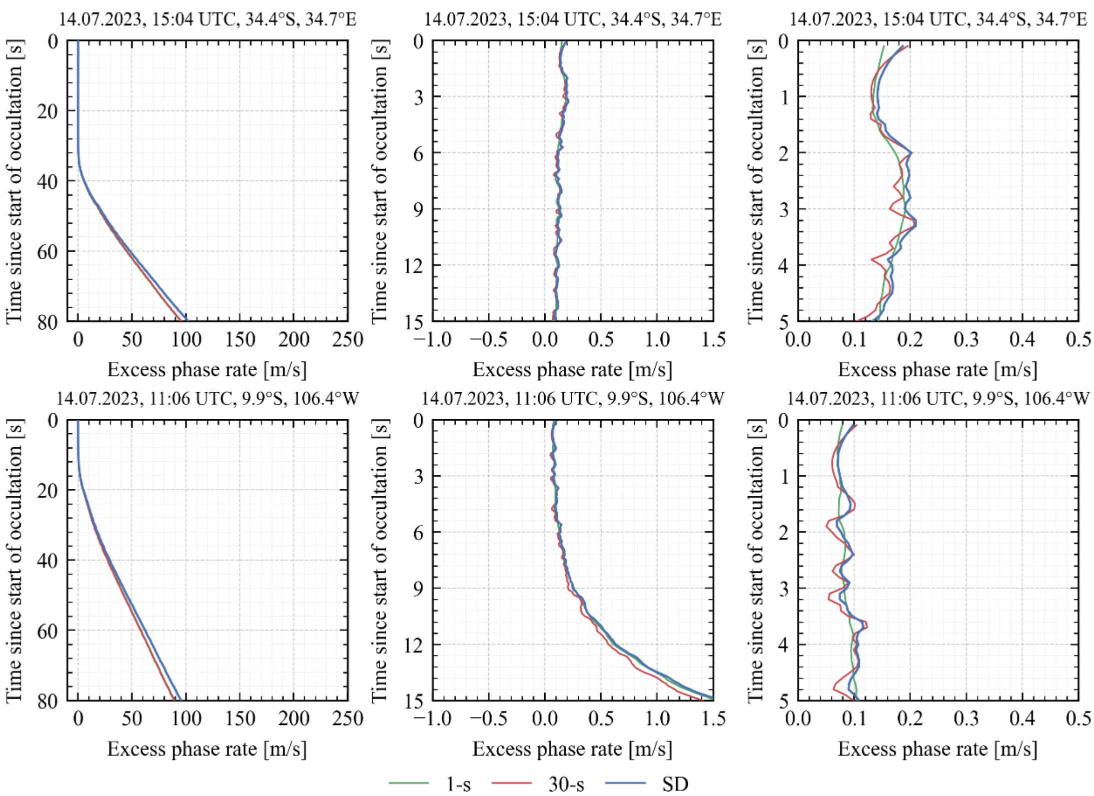

Figure 4: Excess phase rate corresponding to three clock correction schemes (1-s, 30-s, and SD) for two representative FY-3E RO events (first row and second row). Plots from left to right display excess phase rate calculated over different time intervals.

Figure 5 quantitatively presents the systematic differences and corresponding standard deviations of excess phase rate derived from the three proposed processing schemes, 1-s UD minus SD, 30-s UD minus SD, and 1-s UD minus 30-s UD. To facilitate detailed visual inspection and highlight the subtle discrepancy in key altitude layers, enlarged subplots focusing on

https://doi.org/10.5194/egusphere-2026-5629
Preprint. Discussion started: 25 September 2026

the altitude range of 40-60 km are provided. Such comparison can help to separate two dominant error sources affecting RO retrieval, i.e., differences between UD scheme and SD scheme, and the differences between different clock interpolation resolutions. Statistical results show that differences between 1-s UD and SD schemes yields the smallest systematic differences and standard deviations, followed by the differences between the 1-s UD and 30-s UD schemes. In contrast, the differences between the 30-s UD and SD schemes are the largest. These results indicate that the 1-s UD scheme and the SD scheme can both be robust in reducing clock errors and have positive impacts on RO retrievals. Benefiting from the high-temporal-resolution interpolation of 1-s receiver clock correction products, the 1-s UD scheme can better capture the rapid short-term variations of satellite-receiver clock offsets. This superiority has the potential to effectively mitigate clock-induced retrieval errors and thereby improving the overall retrieval performance and stability of final RO atmospheric products.

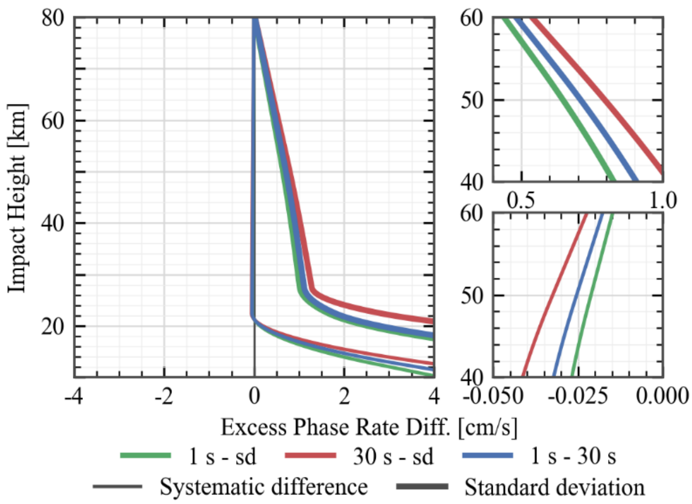

Figure 5: Systematic differences and standard deviations of excess phase rate differences among the 1-s, 30-s, and SD processing schemes. The main panel presents results over the full altitude range. The upper-right and lower-right panels show enlarged views of standard deviations and systematic differences within the 40-60 km altitude ranges, respectively.

Figure 6 shows the statistical errors of ionosphere-corrected bending angle profiles obtained from the three clock correction schemes. Globally, systematic differences of all three schemes are consistent below 40 km and standard deviations of all the three approaches are overall consistent below 50 km. Within the altitude range of 40-60 km, the 1-s scheme exhibits distinct advantages over the other two methods. On a global scale, the systematic differences of the 1-s scheme are approximately 3% smaller than those of the 30-s scheme and 1% smaller than those of the SD scheme. In other regions, the 1-s scheme also reveal consistent advantages than the other two schemes. The most prominent improvements occur in the 20°S-60°S, 20°S-20°N, and 60°N-90°N latitude bands, where its errors are reduced by over 5% relative to the other two schemes. A comparison between the SD and 30-s schemes reveals that the SD method produces smaller systematic deviations across most geographic regions, with the only exception being the latitude zone of 20°S-60°S. At altitudes ranging from 40 to 60 km within this latitudinal band, systematic differences of the SD scheme rise drastically and are much larger than that of the

https://doi.org/10.5194/egusphere-2026-5629
Preprint. Discussion started: 25 September 2026

other two methods. This anomaly is most probably attributed to noises of several individual atmospheric profiles, where noises get magnified during SD scheme. In terms of standard deviations, values of the 1-s scheme are consistently comparably or smaller than the other two schemes. In the tropical and the southern hemisphere polar regions, standard deviations of the 1-s method are smaller than the other two approaches, demonstrating superior stability in these specific areas. Below 45 km altitude, the SD and 30-s approaches produce overall comparable results. Specifically, the 30-s scheme achieves better performance in the 60°S-90°S and 20°S-20°N regions, whereas the SD scheme outperforms its counterpart in the 60°N-90°N zone.

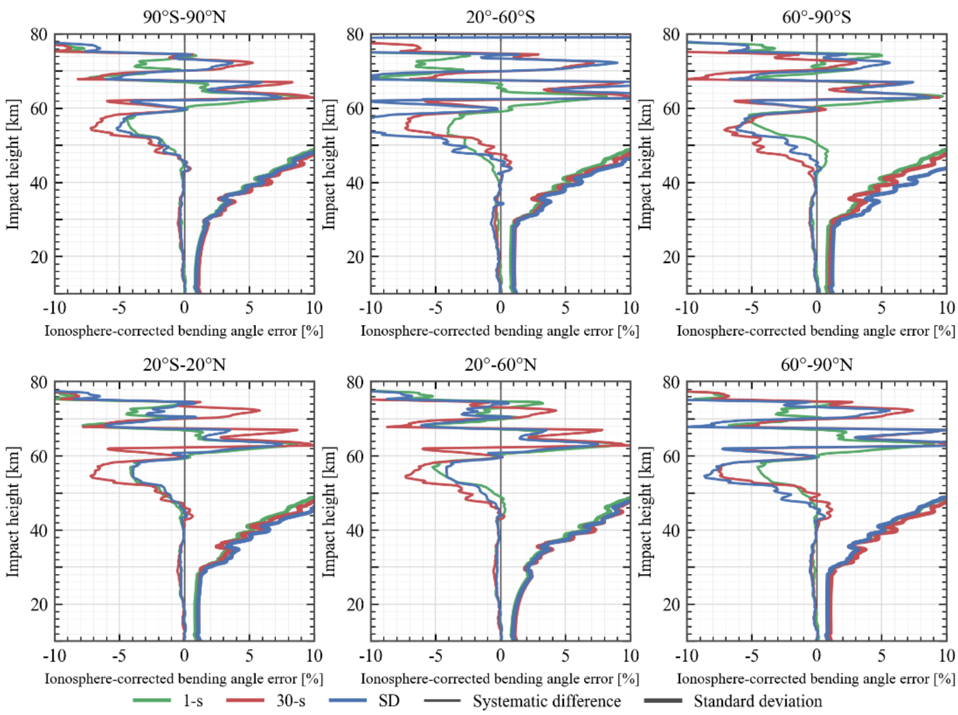

Figure 6: Statistical errors of ionosphere-corrected bending angles from three clock correction strategies, the 1-s correction, the 30-s correction, and the SD schemes. Statistical errors in six latitudinal bands are shown, i.e., the global domain (90°S-90°N), Southern Hemisphere mid-latitudes (20°S-60°S), Northern Hemisphere mid-latitudes (20°N-60°N), Southern Hemisphere polar region (60°S-90°S), Northern Hemisphere polar region (60°N-90°N), and the tropical zone (20°S-20°N).

Above 60 km, statistical errors are too noisy for characterization. Therefore, we calculate the biases and corresponding noises from 65 km to 80 km for further analysis (Li et al., 2026; Pirscher, 2010). Figure 7 presents bending angle biases and noise estimates derived from three different clock correction schemes for individual RO events over three selected days, with the corresponding mean biases and noise magnitudes annotated in the plot. Overall, the 1-s and SD schemes yield bending angle biases and noise at comparable error levels. Systematic differences of individual biases are mostly within ±2 μrad and noises are mostly within 3 μrad. In contrast, both biases and noise for the 30-s scheme are noticeably larger than those of the other two schemes with biases mostly within ±4 μrad and noises mostly within 5 μrad. In terms of mean bias, the 1-s

https://doi.org/10.5194/egusphere-2026-5629
Preprint. Discussion started: 25 September 2026

scheme exhibits the smallest value approximately 0.06 μrad, followed by the SD scheme at roughly 0.09 μrad, while the 30-s scheme produces the largest mean bias of about 0.13 μrad. This indicates that the 1-s clock correction strategy introduces the minimal observational bias among the three configurations. For noise performance, the SD scheme achieves a noise magnitude of 0.71, the 1-s scheme yields a value of 0.81, and the standard deviation associated with the 30-s scheme is markedly larger than the other two strategies. This indicates that the 1-s and SD schemes exhibit smaller systematic differences relative to the ERA5 reanalysis dataset and corresponding smaller standard deviations, whereas the 30-s scheme yields notably larger values for both values. Such errors will propagate downwards to lower altitude levels in refractivity and dry temperature which should be kept in mind for later analysis.

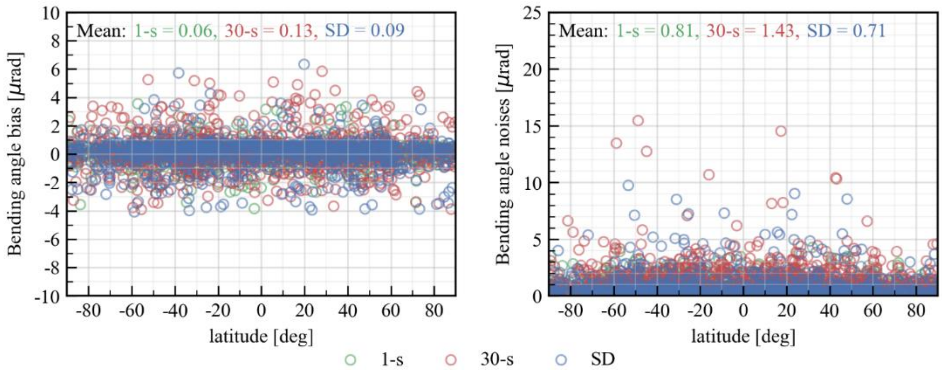

Figure 7: Latitudinal distributions of bending angle biases and noise for the 1-s, 30-s, and SD processing schemes for the period 14-16 July 2023. Mean bias and noise values for each scheme are annotated in the respective subpanels.

Figure 8 illustrates the statistical errors of optimized bending angles, with an identical panel layout to Fig. 6. Benefiting from statistical optimization, the systematic deviations of optimized bending angles are far more stable and smoother compared with ionosphere-corrected bending angles. Similar to ionosphere-corrected bending angles, the systematic differences derived from all three schemes are overall consistent below 40 km. However, evident distinctions emerge in standard deviations within the same altitude range. The 1-s method outperforms the other two schemes, with values are about 1-2% smaller than the other two schemes below 40 km. When comparing the SD and 30-s schemes, SD yields generally smaller standard deviations except within the 60°S-90°S latitudinal band.

Within the altitude layer of 40-60 km, the overall performance of the three approaches is similar to that of ionosphere-corrected bending angles. The 1-s scheme performs the best, with systematic differences are smallest than the other two schemes over all the latitude bands. Globally, systematic differences of the 1-s scheme are about 2% smaller than the SD scheme and are about 3% smaller than the 30-s scheme. The largest improvements are found in the band of 20°S-60°S and 60°N-90°N with systematic differences are more than 5% smaller than the other two schemes at some altitude levels. Comparison between SD and the 30-s scheme illustrates superior results in most regions except the 20°S-60°S band. Best performance is found in the tropical band, with systematic differences of SD approach are close to 1-s approach, and the values are more than 3% smaller than the 30-s approach. In the 20°S-60°S band, systematic differences of the SD approach

https://doi.org/10.5194/egusphere-2026-5629
Preprint. Discussion started: 25 September 2026

again distinctly much larger than the other two schemes in the altitude range between 40-60 km (see Fig. 6 also). This is also related to the noises of several individual RO events which were amplified by the SD scheme as discussed above.

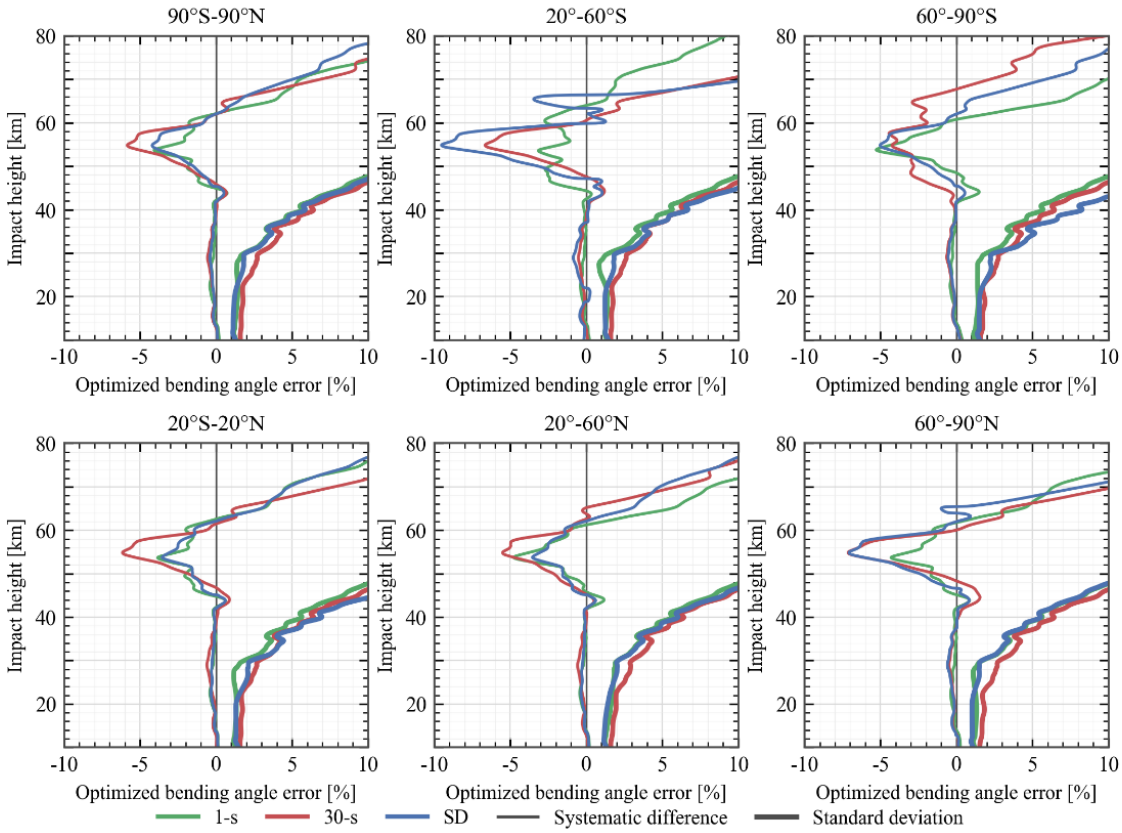

Figure 8: Statistical errors of statistically optimized bending angles derived from three clock correction strategies: 1-s correction, 30-s
280 correction, and SD schemes. Subpanel layout is identical to Fig. 6.

As for standard deviations, values from the 1-s UD scheme are overall approximately 1% smaller than those from the other two schemes, demonstrating the stability of the 1-s UD scheme. When comparing the 1-s UD and SD schemes, their standard deviations are generally comparable over the Northern Hemisphere and tropics, suggesting that the SD scheme is robust for mitigating clock errors in these regions. A comparison between the 30-s UD and SD schemes reveals that the SD scheme also outperforms the 30-s UD scheme in most regions. This implies that the UD scheme with a lower sampling rate yields poorer performance in clock-error reduction relative to the SD scheme.

In summary, the 1-s UD strategy provides the best performance among the three processing schemes, followed by the SD scheme, and then the 30-s UD scheme. For both ionosphere-corrected and statistically optimized bending angle products, the most remarkable performance of 1-s scheme is found in the 40-60 km upper stratosphere. The degraded retrieval quality of the 30-s UD scheme is predominantly driven by large interpolation errors inherent to its low-temporal resolution clock correction products. The onboard LEO receiver clock of FY-3E GNOS-II features distinct short-timescale fluctuations that

https://doi.org/10.5194/egusphere-2026-5629
Preprint. Discussion started: 25 September 2026

linear interpolation of sparse 30-s clock samples cannot fully recover. The RMS offsets between 1-s clock corrections and interpolated 30-s clock time series are 0.098 ns for the forward receiver and 0.092 ns for the backward receiver, with maximum residuals surpassing 0.2 ns (Figs. 2 and 3). A 0.2 ns clock residual corresponds to a slant range error of roughly 6 cm, accounting for nearly one-third of the GPS L1 carrier wavelength. In UD processing workflows, these clock residuals contaminate excess phase observables, which further influences on excess phase rate computations and downstream bending angle inversion. By contrast, high-resolution 1-s clock corrections align perfectly with the occultation sampling cadence, precisely resolving rapid short-term clock fluctuations and drastically cutting interpolation residuals. This advantage efficiently mitigates phase noise and yields smoother bending angle vertical profiles.

Furthermore, the degraded quality of SD schemes mainly arises from additional noise and residual biases originating from the observation link of the reference satellite. While introducing a reference-satellite link can mitigate residual ionospheric errors to a certain degree, it also brings in new error sources. Unmodeled measurement noise along the reference link, together with unremoved systematic offsets, will propagate into the final clock products and degrade the quality of correction results. For this reason, the overall performance of the SD strategy is poorer than the 1-s scheme, especially under conditions with prominent short-timescale clock fluctuations for LEO receivers.

At altitudes above 60 km, residual ionospheric errors introduce substantial noise across all three correction strategies, increasing the dispersion of bending angle systematic differences. Therefore, clock-correction-related influences are no longer among the dominant error sources. Nevertheless, a consistent hierarchy remains evident: the 1-s approach produces the minimal systematic differences in bending angle, the SD method lies in the middle, and the 30-s approach exhibits the largest deviations (see Fig. 7). Standard deviations of both 1-s UD and SD schemes are comparable. These findings indicate that RO profile quality above 60 km can also be improved by adopting higher-accuracy clock-correction schemes.

3.3 Refractivity and dry temperature

Figure 9 presents the statistical errors of refractivity. Globally, the 1-s scheme outperforms the other two schemes: its systematic deviations are approximately 0.5% smaller than the other two schemes at altitudes between 40 km and 60 km, and its standard deviations are reduced by 1%-2% relative to the other schemes. In the tropics and Northern Hemisphere, the 1-s method also shows prominent advantages below 60 km, with around a 1% reduction in systematic differences within the 40-60 km layer. Residual ionospheric errors and observational noise are considerable but not dominant in this altitude range, so both the 1-s and SD schemes are capable of accurately extracting neutral atmospheric information. Above 60 km, residual ionospheric errors become the dominant error source, leading to comparable systematic differences across all three schemes. In terms of standard deviation, the 1-s scheme maintains the best stability with the minimum error magnitude; the SD scheme ranks second, while the standard deviation of the 30-s scheme is roughly 2% larger than the other two retrievals.

https://doi.org/10.5194/egusphere-2026-5629
Preprint. Discussion started: 25 September 2026

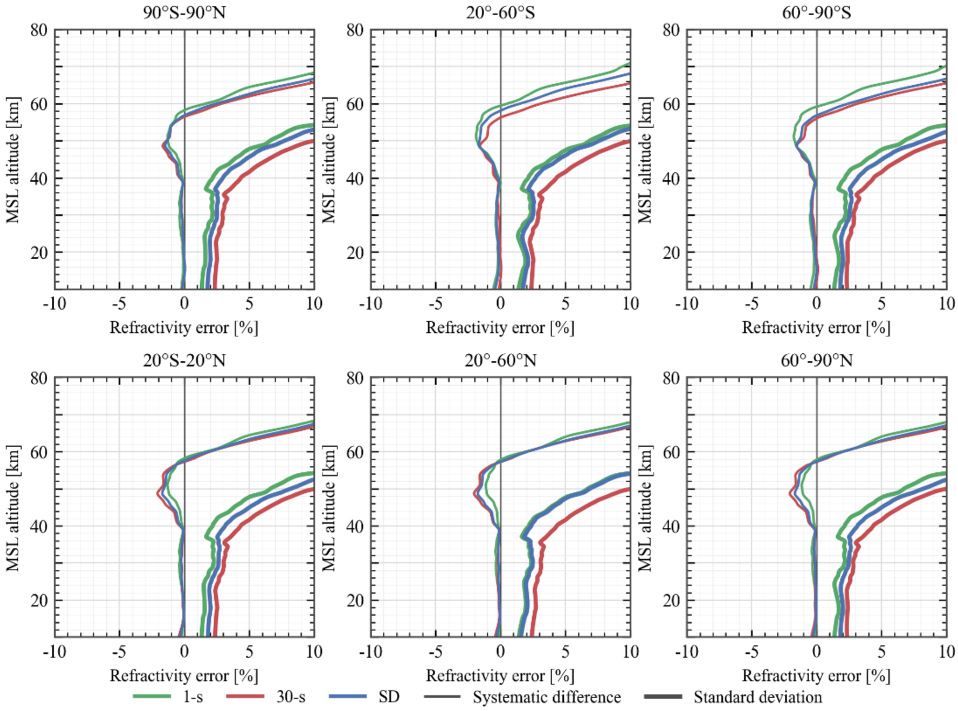

Figure 9: Statistical errors of refractivity derived from three clock correction strategies: 1-s correction, 30-s correction, and SD schemes. Subpanel layout is identical to Figs. 6 and 8.

In terms of latitudinal dependence, the 1-s approach achieves the best performance particularly in the tropical zone and Northern Hemisphere polar areas, delivering distinctly smaller systematic differences and standard deviations, followed sequentially by the SD scheme and the 30-s scheme. Among all latitudinal bands, the tropics and Northern Hemisphere suffer from more severe residual ionospheric disturbances, which mainly originate from equatorial ionospheric irregularities, plasma bubbles and intensified vertical gradients of electron density. Benefiting from high temporal resolution sampling, the 1-s strategy can fully track phase variations and thus realize more precise correction of ionospheric errors. By contrast, the SD sampling framework tends to magnify residual ionospheric perturbations. As a result, the SD scheme introduces markedly larger systematic differences than the 1-s method under disturbed tropical ionospheric environments.

Figure 10 quantifies the statistical errors of dry temperature products inverted via the three sampling strategies. The 1-s scheme continues to deliver evident performance improvements for dry temperature retrieval, although the magnitude of its advantage is weakened relative to those observed for bending angle and refractivity. This attenuation primarily arises from the inherent smoothing effect introduced during hydrostatic integration in the temperature retrieval chain, which suppresses fine-scale error differences inherited from the upper-level bending angle observations. Even so, the superiority of the 1-s method is clearly reflected in standard deviation, demonstrating that dry temperature vertical profiles obtained from the 1-s sampling mode possess stronger stability and less random noise compared with the other two alternatives.

https://doi.org/10.5194/egusphere-2026-5629
Preprint. Discussion started: 25 September 2026

From a global perspective, the systematic differences of the 1-s and SD schemes are generally comparable, and both reduce systematic deviations by approximately 0.5 K relative to the 30-s scheme in the 40 to 60 km altitude range. When it comes to random error characterized by standard deviation, the 1-s approach outperforms the remaining two methods across most altitude layers and latitudinal zones. Specifically, its standard deviation is roughly 1% smaller than that of the SD scheme and around 2% smaller than the values yielded by the 30-s scheme.

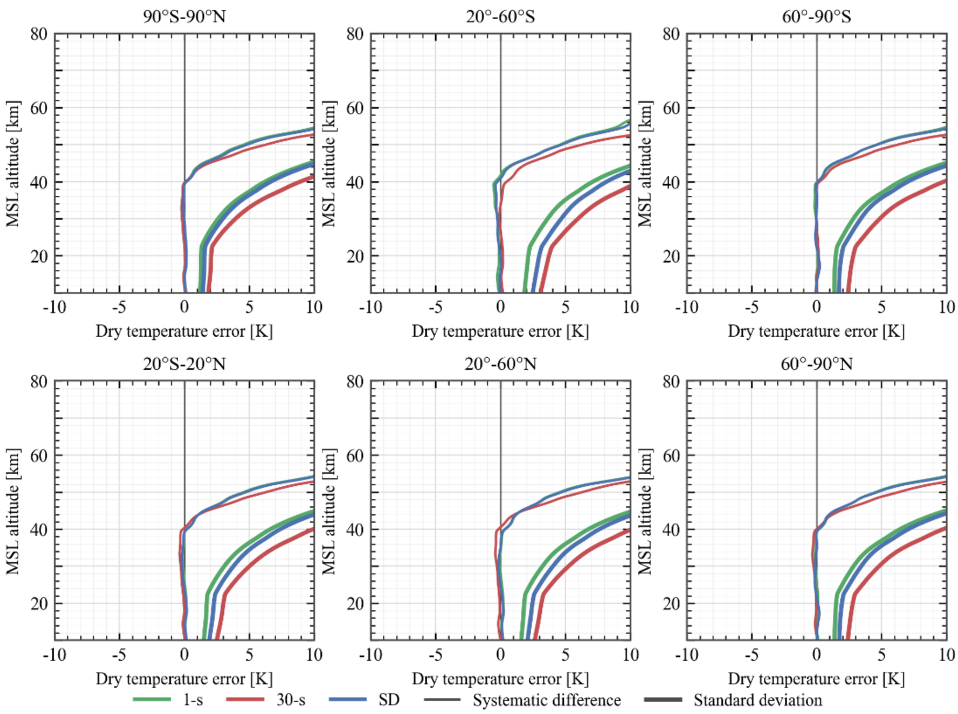

Figure 10: Statistical errors of dry temperature derived from three clock correction strategies: 1-s correction, 30-s correction, and SD schemes. Subpanel layout is identical to Figs. 6, 8 and 9.

4 Conclusions

This work investigates the performance of three clock correction schemes, i.e., 1-s correction, 30-s correction and SD schemes on RO retrievals of FY-3E GNOS-II receivers. We first calculate clock corrections for the three schemes to compute RO excess phase, then apply the ROPP processing package to generate vertical profiles of bending angle, refractive index and dry atmospheric temperature. ERA5 reanalysis fields are used as the reference dataset for validation. By computing the systematic differences and corresponding standard deviation of RO retrievals within six distinct latitude bands, we characterize the overall error magnitude of the three schemes and their latitudinal dependence.

In summary, the 1-s sampling scheme exhibits superior performance relative to the remaining two approaches. The SD method comes second, and the 30-s UD approach delivers the lowest accuracy among the three. In terms of bending angle retrievals, the most sensitive error reduction can be observed in the altitude range of 40-60 km. Globally speaking, the systematic deviations of the 1-s scheme are roughly 3% smaller than those of the 30-s scheme and 1% smaller than the SD scheme. Furthermore, the 1-s approach exhibits consistent advantages across all latitudinal regions. Its performance is most notable in the latitudinal bands of 20°S-60°S, 20°S-20°N and 60°N-90°N, where its errors decrease by more than 5% compared with 30-s UD and/or SD schemes. A comparison of the SD and 30-s schemes shows SD yields smaller systematic deviations over most regions, except for the 20°S-60°S latitude band. Within this zone at 40-60 km altitude, SD exhibits drastically enlarged systematic biases likely caused by amplified noise from individual atmospheric profiles. In terms of standard deviations, values of the 1-s scheme are consistently comparably or smaller than the other two schemes. The SD and 30-s approaches produce largely comparable results.

At altitudes above 60 km, the 1-s method shows the smallest discrepancies against ERA5 reanalysis data, followed by the SD scheme and then the 30-s scheme. This indicates that the 1-s scheme can still have obvious positive impacts at altitudes where residual ionospheric errors dominate. In terms of standard deviation, the 1-s UD and SD schemes yield comparable values. This indicates that both schemes are robust for mitigating clock errors at high altitudes. In contrast, the 30-s scheme suffers from larger systematic differences and standard deviations than the remaining two schemes.

The errors remained in bending angle will propagate downwards to lower altitude levels in refractivity and dry temperature. Globally, the refractivity systematic differences of the 1-s scheme are approximately 0.5% smaller than those of the other two methods. In terms of refractivity standard deviations, the 1-s approach outperforms the SD scheme by nearly 1% and the 30-s scheme by 2%. In terms of latitudinal characteristics, the 1-s scheme delivers optimal performance in the Northern Hemisphere and tropical regions, demonstrating its superior robustness under strong ionospheric activity. This is consistent with its better performance in bending angle retrievals. For dry temperature profiles, however, the advantages of the 1-s scheme are diminished by the smoothing effect of hydrostatic integration. All three schemes exhibit generally consistent systematic temperature differences below 40 km. Nevertheless, the 1-s scheme yields the smallest standard deviations, followed sequentially by the SD and 30-s schemes, which demonstrates its reliable and stable retrieval capability.

This study proves that the clock onboard FY-3E satellite GNOS-II RO receiver exhibits sufficient stability and can provide stable high-precision clock products. The UD clock-correction scheme shows great potential for further improving the quality of FY-3E RO profiles within the middle stratosphere. Nevertheless, it requires high-temporal-resolution clock correction terms, such as the 1-s clock corrections. The results here can provide support for future operational processing and archive reprocessing of all Fengyun GNOS-II RO datasets.

Code and data availability

The custom scripts, intermediate data, and plot data generated in this study are available from the corresponding author upon reasonable request. The FY-3E GNOS-II RO data are available from the National Satellite Meteorological Centre (NSMC) Data Service via https://data.nsmc.org.cn. The ERA5 reanalysis data used for validation are available from the Copernicus Climate Data Store via https://cds.climate.copernicus.eu (Hersbach et al., 2020). The GNSS precise orbit products and 30-s satellite clock corrections used for FY-3E orbit determination are available from the Center for Orbit Determination in Europe (CODE) via https://www.aiub.unibe.ch/download/CODE (Dach et al., 2024). The GNSS precise orbit and clock products used for transmitter-side clock correction are available from the International GNSS Service (IGS) via https://www.igs.org/products (Johnston et al., 2017).

Author contributions

Xinyu Zhang conducted the algorithm design, data processing, experiments, result analysis, figure preparation, and manuscript writing. Wenwu Ding, as the corresponding author, proposed the research idea, provided advice and guidance on algorithm design, result analysis, and figure preparation, and contributed to manuscript revision. Xiangguang Meng contributed to the calculation of LEO 1-s clock corrections, provided raw data, and assisted with figure preparation. Ying Li contributed to data analysis, figure preparation, and manuscript revision. Yan Liu contributed to data collection, validation, and manuscript writing. Yunbin Yuan contributed to algorithm design, validation, and manuscript revision. All authors reviewed and approved the final manuscript.

Competing interests

The authors declare that they have no conflict of interest.

Acknowledgements

The authors acknowledge the European Centre for Medium-Range Weather Forecasts (ECMWF) and the Copernicus Climate Data Store for supplying ERA5 reanalysis data. Gratitude is also extended to the Center for Orbit Determination in Europe (CODE), the International GNSS Service (IGS), and the Radio Occultation Meteorology Satellite Application Facility (ROM SAF) for providing the datasets and software utilized throughout this study. ChatGPT was used for language polishing and editorial refinement. The authors reviewed and edited the output and take full responsibility for the published article.

Financial support

The research at the Academy of Precision Measurement Science and Technology, Chinese Academy of Sciences (APM, Wuhan, China) was supported by the National Natural Science Foundation of China (Grant No. 42474063), the National Key Research and Development Program (Grant No. 2023YFA1009100), and the Strategic Talent Cultivation Project of Hubei Province (Grant Nos. KJCXRC202400130 and 2024DJA016). The research at the National Space Science Center, Chinese

Academy of Sciences (NSSC, Beijing, China) was supported by the National Natural Science Foundation of China (Grant No. U2542214).

References

Angerer, B., Ladstädter, F., Scherllin-Pirscher, B., Schwärz, M., Steiner, A. K., Foelsche, U., and Kirchengast, G.: Quality aspects of the Wegener Center multi-satellite GPS radio occultation record OPSv5.6, Atmos. Meas. Tech., 10, 4845–4863, https://doi.org/10.5194/amt-10-4845-2017, 2017.

Anthes, R.: Exploring Earth's atmosphere with radio occultation: Contributions to weather, climate and space weather, Atmos. Meas. Tech., 4, 1077–1103, https://doi.org/10.5194/amt-4-1077-2011, 2011.

Beyerle, G., Schmidt, T., Michalak, G., Heise, S., Wickert, J., and Reigber, C.: GPS radio occultation with GRACE: Atmospheric profiling utilizing the zero difference technique, Geophys. Res. Lett., 32, L13806, https://doi.org/10.1029/2005GL023109, 2005.

Bosilovich, M. G., Kennedy, J., Dee, D., Allan, R., and O'Neill, A.: On the reprocessing and reanalysis of observations for climate, in: Climate science for serving society: Research, modeling and prediction priorities, Springer, 51–71, 10.1007/978-94-007-6692-1_3, 2013.

Cucurull, L. and Derber, J.: Operational implementation of COSMIC observations into NCEP's global data assimilation system, Weather Forecast., 23, 702–711, https://doi.org/10.1175/2008WAF2007070.1, 2008.

Culverwell, I., Lewis, H., Offiler, D., Marquardt, C., and Burrows, C.: The radio occultation processing package RoPP, Atmos. Meas. Tech., 8, 1887–1899, https://doi.org/10.5194/amt-8-1887-2015, 2015.

Dach, R., Lutz, S., Walser, P., and Fridez, P.: Bernese GNSS Software Version 5.2. User manual, Astronomical Institute, University of Bern, [Software]. Bern Open Publishing. [code], https://doi.org/10.7892/boris.72297, 2015.

Dach, R., Schaer, S., Arnold, D., Brockmann, E., Kalarus, M. S., Lasser, M., Stebler, P., and Jäggi, A.: CODE ultra-rapid product series for the IGS, Astronomical Institute, University of Bern, 10.48350/197027, https://www.aiub.unibe.ch/download/CODE, 2024.

Fjeldbo, G., Kliore, A. J., and Eshleman, V. R.: The neutral atmosphere of Venus as studied with the Mariner V radio occultation experiments, Astron. J., 76, 123–140, https://doi.org/10.1086/111096, 1971.

Foelsche, U., Scherllin-Pirscher, B., Ladstädter, F., Steiner, A., and Kirchengast, G.: Refractivity and temperature climate records from multiple radio occultation satellites consistent within 0.05%, Atmos. Meas. Tech., 4, 2007–2018, https://doi.org/10.5194/amt-4-2007-2011, 2011.

Guo, S., Zhang, S., Meng, X., Wu, Y., Lou, Y., and Lin, J.: Undifferenced processing of COSMIC-2 radio occultation measurements with 1-Hz LEO clock corrections, GPS Solut., 28, 18, https://doi.org/10.1007/s10291-023-01559-6, 2024.

Hajj, G. A., Kursinski, E., Romans, L., Bertiger, W., and Leroy, S.: A technical description of atmospheric sounding by GPS occultation, Journal of Atmospheric and solar-terrestrial physics, 64, 451–469, https://doi.org/10.1016/S1364-6826(01)00114-6, 2002.

Healy, S. and Eyre, J.: Retrieving temperature, water vapour and surface pressure information from refractive-index profiles derived by radio occultation: A simulation study, Q. J. Roy. Meteor. Soc., 126, 1661–1683, https://doi.org/10.1002/qj.49712656606, 2000.

Hersbach, H.: Global reanalysis: goodbye ERA-Interim, hello ERA5, ECMWF Newsletter, 159, 17–24, https://doi.org/10.21957/vf291hehd7, 2019.

Hersbach, H., Bell, B., Berrisford, P., Hirahara, S., Horányi, A., Muñoz-Sabater, J., Nicolas, J., Peubey, C., Radu, R., and Schepers, D.: The ERA5 global reanalysis, Q. J. Roy. Meteor. Soc., 146, 1999–2049, https://doi.org/10.1002/qj.3803, 2020.

Huang, C.-Y., Kuo, Y.-H., Chen, S.-Y., Terng, C.-T., Chien, F.-C., Lin, P.-L., Kueh, M.-T., Chen, S.-H., Yang, M.-J., and Wang, C.-J.: Impact of GPS radio occultation data assimilation on regional weather predictions, GPS Solut., 14, 35–49, https://doi.org/10.1007/s10291-009-0144-1, 2010.

Hwang, C., Tseng, T.-P., Lin, T., Švehla, D., and Schreiner, B.: Precise orbit determination for the FORMOSAT-3/COSMIC satellite mission using GPS, J. Geod., 83, 477–489, https://doi.org/10.1007/s00190-008-0256-3, 2009.

Innerkofler, J., Kirchengast, G., Schwärz, M., Marquardt, C., and Andres, Y.: GNSS radio occultation excess-phase processing for climate applications including uncertainty estimation, Atmos. Meas. Tech., 16, 5217–5247, https://doi.org/10.5194/amt-16-5217-2023, 2023.

Jaeggi, A., Arnold, D., Weiss, J., and Hunt, D.: Assessment of COSMIC-2 reduced-dynamic and kinematic orbit determination, EGU General Assembly Conference Abstracts, EGU21–12027, https://doi.org/10.5194/egusphere-egu21-12027, 2021.

Johnston, G., Riddell, A., and Hausler, G.: The international GNSS service, in: Springer handbook of global navigation satellite systems, Springer, 967–982, 10.1007/978-3-319-42928-1_33, 2017.

Kang, Z., Tapley, B., Bettadpur, S., Ries, J., Nagel, P., and Pastor, R.: Precise orbit determination for the GRACE mission using only GPS data, J. Geod., 80, 322–331, https://doi.org/10.1007/s00190-006-0073-5, 2006.

Kong, Q., Chen, Y., Fang, W., Wang, G., Li, C., Wang, T., Bai, Q., and Han, J.: Analysis of space-borne GPS data quality and evaluation of precise orbit determination for COSMIC-2 mission based on reduced dynamic method, Remote Sens., 14, 3544, https://doi.org/10.3390/rs14153544, 2022.

Kursinski, E., Hajj, G., Schofield, J., Linfield, R., and Hardy, K. R.: Observing Earth's atmosphere with radio occultation measurements using the Global Positioning System, J. Geophys. Res.-Atmos., 102, 23429–23465, https://doi.org/10.1029/97JD01569, 1997.

Ladstädter, F., Steiner, A., Schwärz, M., and Kirchengast, G.: Climate intercomparison of GPS radio occultation, RS90/92 radiosondes and GRUAN from 2002 to 2013, Atmos. Meas. Tech., 8, 1819–1834, https://doi.org/10.5194/amt-8-1819-2015, 2015.

https://doi.org/10.5194/egusphere-2026-5629
Preprint. Discussion started: 25 September 2026

Li, Y., Kirchengast, G., Scherllin-Pirscher, B., Wu, S., Schwaerz, M., Fritzer, J., Zhang, S., Carter, B., and Zhang, K.: A new dynamic approach for statistical optimization of GNSS radio occultation bending angles for optimal climate monitoring utility, J. Geophys. Res.-Atmos., 118, 13,022–013,040, https://doi.org/10.1002/2013JD020763, 2013.

Li, Y., Kirchengast, G., Scherllin-Pirscher, B., Norman, R., Yuan, Y., Fritzer, J., Schwaerz, M., and Zhang, K.: Dynamic statistical optimization of GNSS radio occultation bending angles: Advanced algorithm and performance analysis, Atmos. Meas. Tech., 8, 3447–3465, https://doi.org/10.5194/amt-8-3447-2015, 2015.

Li, Y., Kirchengast, G., Schwärz, M., Ladstädter, F., and Yuan, Y.: Monitoring sudden stratospheric warmings using radio occultation: a new approach demonstrated based on the 2009 event, Atmos. Meas. Tech., 14, 2327–2343, https://doi.org/10.5194/amt-14-2327-2021, 2021.

Li, Y., Kirchengast, G., Schwaerz, M., and Yuan, Y.-B.: Monitoring sudden stratospheric warmings under climate change since 1980 based on reanalysis data verified by radio occultation, Atmos. Chem. Phys., 23, 1259–1284, https://doi.org/10.5194/acp-23-1259-2023, 2023.

Li, Y., Liu, Y., Ding, W., Liao, M., Huo, X., and Ye, J.: Quality aspects of Fengyun3 D/E radio occultation bending angle products, Atmos. Meas. Tech., 19, 659–678, https://doi.org/10.5194/amt-19-659-2026, 2026.

Liao, M., Healy, S., and Zhang, P.: Processing and quality control of FY-3C GNOS data used in numerical weather prediction applications, Atmos. Meas. Tech., 12, 2679–2692, https://doi.org/10.5194/amt-12-2679-2019, 2019.

Melbourne, W., Davis, E., Duncan, C., Hajj, G., Hardy, K., Kursinski, E., Meehan, T., Young, L., and Yunck, T.: The application of spaceborne GPS to atmospheric limb sounding and global change monitoring, 1994.

Padovan, S., Von Engeln, A., Paolella, S., Andres, Y., Galley, C. R., Notarpietro, R., Rivas Boscan, V., Sancho, F., Martin Alemany, F., and Morew, N.: Observed impact of the GNSS clock data rate on radio occultation bending angles for Sentinel-6A and COSMIC-2, Atmos. Meas. Tech., 3217–3228, https://doi.org/10.5194/amt-18-3217-2025, 2025.

Parker, W. S.: Reanalyses and observations: What's the difference?, Bull. Am. Meteorol. Soc., 97, 1565–1572, https://doi.org/10.1175/BAMS-D-14-00226.1, 2016.

Pirscher, B.: Multi-satellite climatologies of fundamental atmospheric variables from Radio Occultation and their validation, PhD thesis, University of Graz, Graz, Austria, 218 pp., 2010.

ROM SAF: ROPP-11.3 Release Notes and Installation Guide, Release notes and installation guide Version 11.3, Radio Occultation Meteorology Satellite Application Facility, https://rom-saf.eumetsat.int/ROPP_Release_Notes.pdf, 2024.

Schreiner, W., Rocken, C., Sokolovskiy, S., and Hunt, D.: Quality assessment of COSMIC/FORMOSAT-3 GPS radio occultation data derived from single-and double-difference atmospheric excess phase processing, GPS Solut., 14, 13–22, https://doi.org/10.1007/s10291-009-0132-5, 2010.

Schreiner, W., Sokolovskiy, S., Hunt, D., Rocken, C., and Kuo, Y.-H.: Analysis of GPS radio occultation data from the FORMOSAT-3/COSMIC and Metop/GRAS missions at CDAAC, Atmos. Meas. Tech., 4, 2255–2272, https://doi.org/10.5194/amt-4-2255-2011, 2011.

Simmons, A., Soci, C., Nicolas, J., Bell, B., Berrisford, P., Dragani, R., Flemming, J., Haimberger, L., Healy, S., and Hersbach, H.: Global stratospheric temperature bias and other stratospheric aspects of ERA5 and ERA5. 1, https://doi.org/10.21957/rcxqfmg0, 2020.

Singh, R., Ojha, S. P., Anthes, R., and Hunt, D.: Evaluation and assimilation of the COSMIC-2 radio occultation constellation observed atmospheric refractivity in the WRF data assimilation system, J. Geophys. Res.-Atmos., 126, e2021JD034935, https://doi.org/10.1029/2021JD034935, 2021.

Sokolovskiy, S.: Statistical optimization approach for GPS/MET data inversion, URSI GPS/MET workshop, 1996,

Steiner, A., Lackner, B., Ladstädter, F., Scherllin-Pirscher, B., Foelsche, U., and Kirchengast, G.: GPS radio occultation for climate monitoring and change detection, Radio Sci., 46, 1–17, https://doi.org/10.1029/2010RS004614, 2011.

Steiner, A. K., Ladstädter, F., Ao, C. O., Gleisner, H., Ho, S.-P., Hunt, D., Schmidt, T., Foelsche, U., Kirchengast, G., and Kuo, Y.-H.: Consistency and structural uncertainty of multi-mission GPS radio occultation records, Atmos. Meas. Tech., 13, 2547–2575, https://doi.org/10.5194/amt-13-2547-2020, 2020.

Teng, H. F., Kuo, Y. H., and Done, J. M.: Potential impacts of radio occultation data assimilation on forecast skill of tropical cyclone formation in the western North Pacific, Geophys. Res. Lett., 50, e2021GL096750, https://doi.org/10.1029/2021GL096750, 2023.

Weiss, J.-P.: Recent precise orbit determination results for the COSMIC-2 mission, 43rd COSPAR Scientific Assembly. Held 28 January-4 February, 43, 2337, 2021.

Wickert, J., Reigber, C., Beyerle, G., König, R., Marquardt, C., Schmidt, T., Grunwaldt, L., Galas, R., Meehan, T. K., and Melbourne, W. G.: Atmosphere sounding by GPS radio occultation: First results from CHAMP, Geophys. Res. Lett., 28, 3263–3266, https://doi.org/10.1029/2001GL013117, 2001.

Wickert, J., Beyerle, G., Hajj, G. A., Schwieger, V., and Reigber, C.: GPS radio occultation with CHAMP: Atmospheric profiling utilizing the space-based single difference technique, Geophys. Res. Lett., 29, 28–21–28–24, https://doi.org/10.1029/2001GL013982, 2002.

Wickert, J., Beyerle, G., König, R., Heise, S., Grunwaldt, L., Michalak, G., Reigber, C., and Schmidt, T.: GPS radio occultation with CHAMP and GRACE: A first look at a new and promising satellite configuration for global atmospheric sounding, Annales Geophysicae, 653–658, https://doi.org/10.5194/angeo-23-653-2005, 2005,

Xia, P., Ye, S., Jiang, K., and Chen, D.: Estimation and evaluation of COSMIC radio occultation excess phase using undifferenced measurements, Atmos. Meas. Tech., 10, 1813–1821, https://doi.org/10.5194/amt-10-1813-2017, 2017.

Yang, M., Meng, X., Tian, H., Sun, Y., Du, Q., Bai, W., Wang, B., Wang, X., Hu, P., and Tan, G.: First Galileo Single-Frequency Occultation Process and Precision Analysis of FengYun3E, Remote Sens., 15, 4410, https://doi.org/10.3390/rs15184410, 2023a.

Yang, S. C., Chen, S. H., and Chang, C. C.: Understanding the impact of assimilating FORMOSAT-7/COSMIC-2 radio occultation refractivity on tropical cyclone genesis: Observing system simulation experiments using Hurricane Gordon (2006) as a case study, Q. J. Roy. Meteor. Soc., 149, 1293–1318, https://doi.org/10.1002/qj.4455, 2023b.

https://doi.org/10.5194/egusphere-2026-5629
Preprint. Discussion started: 25 September 2026

Yao, J., Weiss, J.-P., and VanHove, T.: Impacts of high rate GNSS satellite clock estimation on radio occultation bending angle retrievals: preliminary report, Proceedings of the 2023 International Technical Meeting of The Institute of Navigation, 995–1001, https://doi.org/10.33012/2023.18621, 2023.

Yao, J., Ko, Y.-C., Weiss, J.-P., VanHove, T., and Schreiner, W. S.: Reducing radio occultation uncertainty using high-rate GNSS satellite clock estimation, Measurement Science and Technology, 36, 126306, https://doi.org/10.1088/1361-6501/ae234f, 2025.

Zhang, B., Ho, S.-p., Cao, C., Shao, X., Dong, J., and Chen, Y.: Verification and validation of the COSMIC-2 excess phase and bending angle algorithms for data quality assurance at STAR, Remote Sens., 14, 3288, https://doi.org/10.3390/rs14143288, 2022.